Research Article Vol. 35, No. 10 / October 2018 / Journal of the Optical Society of America B 2443

Journal of the Optical Society of America B

OPTICAL PHYSICS

Optical response induced by bound states in the continuum in arrays of dielectric spheres

E. N. Bulgakov[1,2] and D. N. Maksimov[1,2,*]

[1]Reshetnev Siberian State University of Science and Technology, 660037, Krasnoyarsk, Russia
[2]Kirensky Institute of Physics, Federal Research Center KSC SB RAS, 660036, Krasnoyarsk, Russia
*Corresponding author: mdn@tnp.krasn.ru

Received 6 June 2018; revised 16 August 2018; accepted 16 August 2018; posted 17 August 2018 (Doc. ID 334535); published 11 September 2018

We consider an optical response induced by bound states in the continuum (BICs) in arrays of dielectric spheres. By combining the quasi-mode expansion technique with coupled mode theory (CMT), we put forward a theory of the optical response by high-Q resonance surrounding BICs in momentum space. The central results are analytical expressions for the CMT parameters, which can be easily calculated from the eigenfrequencies and eigenvectors of the interaction matrix of the scattering systems. The results obtained are verified in comparison against exact numerical solutions to demonstrate that the CMT approximation is capable of reproducing Fano features in the spectral vicinity of the BIC. Based on the quasi-mode expansion technique, we derived the asymptotic scaling law for the CMT parameters in the vicinity of the Γ-point. It is rigorously demonstrated that the linewidth in the CMT approximation exhibits different asymptotic behavior depending on the symmetry of the BIC.

https://doi.org/10.1364/JOSAB.35.002443

1. INTRODUCTION

The phenomenon of light localization is of paramount importance in modern science and technology [1]. One of the physical phenomena leading to the localization of light is optical bound states in the continuum (BICs) [2]. BICs are localized eigenmodes of Maxwell's equation embedded into the continuous spectrum of the scattering states, i.e., source-free solutions that do not radiate into the far-zone, albeit outgoing waves with the same frequency and wave vector are allowed in the surrounding medium. In view of time reversal symmetry, this implies that an ideal BIC is invisible from the far-zone because it is also decoupled from any incident wave impinging onto the BIC supporting structure. At first glance, this renders BICs totally useless for practical purposes. However, if the scattering problem is granted an extra dimension by introducing a control parameter, one can immediately see that the traces of BICs emerge in the scattering spectrum as narrow Fano features once the control parameter is detuned from the BIC-point [3–7]. The collapsing Fano feature is generally seen as a precursor of BIC not only in optics but in the fields of acoustics [8] and quantum mechanics [9]. The emergence of Fano resonance is associated with critical light enhancement [10,11], which paves the way toward important applications for light–matter interaction, including lasing [12–14], harmonics generation [15,16], and bio-sensing [17].

Among various setups, BICs are known to exist in periodic dielectric structures [18–29]. In that case, any eigenmode of Maxwell's equations is characterized by its Bloch wavenumber β with respect to a certain axis of periodicity. Thus, the periodicity by itself quite naturally offers the wavenumber as a control parameter for optical response. Two classes of eigenmodes are generally discriminated in periodic structures. The eigenmodes with frequency below the line of light $\omega = c\beta$ are always localized due to the total internal reflection. In contrast, the eigenmodes with frequency above the line of light are normally leaky, i.e., radiate to the outer space [30]. In that context, BIC can be seen as exceptional points of the leaky zones in which the far-field radiation from the leaky mode vanishes due to intricate destructive interference between waves radiated from the infinite number of the elementary cells of the periodic structure. The BICs are observed from the dispersion of the leaky-zone Q-factor as the points where the Q-factor diverges to infinity. This implies that, spectrally, any BIC is surrounded by a family by high-Q leaky modes [31,32] with the Q-factor infinitely increasing as β is tuned to the BIC-point.

In this paper, we propose a theory of optical response from such high-Q leaky modes surrounding BICs in linear periodic arrays of dielectric spheres [23]. To construct the theory of the resonant response, two approaches are merged together. The first is a rigorous quasi-mode expansion technique that relies on the bi-orthogonal basis of the interaction matrix of the scattering system [33–38]. The second approach is coupled mode theory (CMT) [39–41], which proved itself as an efficient tool for approximating the resonant response of optical systems.

In what follows, we shall establish a link between the two approaches to provide a clear physical picture in terms of the leaky mode coupling coefficients leading to simple expressions for amplitudes of the scattered waves. We shall reveal the asymptotic behavior of the coupling coefficients in the spectral vicinity of BIC and numerically demonstrate the validity of the proposed approach.

2. SCATTERING THEORY

The system under consideration is an array of dielectric spheres with permittivity $\epsilon = 15$ in air, as shown in Fig. 1. The electromagnetic (EM) field can be found from time-stationary Maxwell's equations:

$$\nabla \times \mathbf{E} = ik_0\mathbf{H}, \qquad \nabla \times \mathbf{H} = -ik_0\epsilon(\mathbf{r})\mathbf{E}, \tag{1}$$

where $\mathbf{H}$ and $\mathbf{E}$ are the magnetic and electric vectors, $\epsilon(\mathbf{r})$ is the dielectric permittivity, and k_0 is the vacuum wavenumber, $k_0 = \omega/c$ with ω is the frequency and c is the speed of light. Note that, throughout this paper, we adopted Gaussian units to comply with the previous publications on the subject [23,42]. In what follows, we set $c = 1$ to measure the frequency in the units of distance. The solution for the EM field scattered by the array could be found by using the method developed by Linton, Zalipaev, and Thompson [42]. According to [42], both $\mathbf{E}$ and $\mathbf{H}$ outside the spheres are written as a series over spherical vector harmonics $\mathbf{N}_l^m(\mathbf{r}), \mathbf{M}_l^m(\mathbf{r})$ in the following forms:

$$\mathbf{E}(\mathbf{r}) = \sum_{j=-\infty}^{\infty} e^{iaj\beta} \sum_{l=m^*}^{\infty} [\overline{a}_l^m \mathbf{M}_l^m(\mathbf{r}_j) + \overline{b}_l^m \mathbf{N}_l^m(\mathbf{r}_j)],$$

$$\mathbf{H}(\mathbf{r}) = -i\sqrt{\epsilon} \sum_{j=-\infty}^{\infty} e^{iaj\beta} \sum_{l=m^*}^{\infty} [\overline{a}_l^m \mathbf{N}_l^m(\mathbf{r}_j) + \overline{b}_l^m \mathbf{M}_l^m(\mathbf{r}_j)], \tag{2}$$

where j is the number of the sphere in the array, a is the distance between the centers of the spheres, $\mathbf{r}_j$ is coordinate vector in the j_{th} sphere reference frame, and $m^* = \max(1, m)$. When the scattering problem is addressed, the EM field is found by solving a set of linear equations [23],

$$\widehat{\mathcal{L}}\mathbf{p} = \mathbf{q}, \tag{3}$$

where $\mathbf{p}$ is the vector of the expansion coefficients of the scattered EM field,

$$\mathbf{p} = \{\overline{a}_l^m, \overline{b}_l^m\}, \tag{4}$$

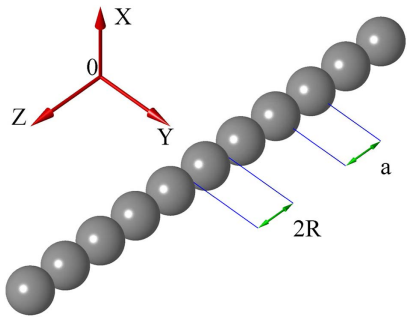

Fig. 1. Array of dielectric spheres of radius R periodically arranged along the z axis with period a.

where $\mathbf{q}$ is the vector of the expansion coefficients of the incident wave,

$$\mathbf{q} = \{c_l^m, d_l^m\}, \tag{5}$$

and $\widehat{\mathcal{L}}$ is the interaction matrix of the scattering system. We spare the reader of the exact, rather cumbersome, expression for $\widehat{\mathcal{L}}$ because it is already given in [23] (and implicitly in the original paper [42]).

Given that matrix $\widehat{\mathcal{L}}$ is a known quantity, we yet have to define vector $\mathbf{q}$. The expression for $\mathbf{q}$ depends on the configuration of the incident EM field. The most obvious choice for probing the resonant response is a monochromatic plane wave. The plane wave is specified by its polarization; a transverse electric (TE) wave has its electric vector orthogonal to the array axis, while, for a transverse magnetic (TM) wave, it is the magnetic vector that is orthogonal to the axis of the array. Importantly, the BICs in arrays of dielectric spheres always have quantized orbital angular momentum (OAM) m [23], which reflects the rotational symmetry of the system. Because OAM is preserved by scattering of the cylindrical waves, the scattering problem for a plane wave can be solved independently for each m. In what follows, we shall only consider scattering in subspace with OAM equal to that of the BIC, having in mind that the response to a plane wave could be found relying on the expansion of a plane wave into cylindrical Bessel functions [43]. As demonstrated in [23], the sharp resonant feature in the spectral vicinity of a BIC is clearly visible in the total scattering cross-section because subspaces with OAM different from that of the BIC provide only a smooth nonresonant background contribution. For each m, the incident TM (TE) wave is defined as

$$E_z^{(m)}(H_z^{(m)}) = \frac{1}{\sqrt{C(\mathbf{k})}} \exp(im\phi + ik_z z) J_m(k_\perp \rho), \tag{6}$$

with

$$k_\perp^2 = k_0^2 - k_z^2, \tag{7}$$

where $\{\rho, \phi, z\}$ are the cylindrical coordinates, k_z is the z component of the wave vector, and $C(\mathbf{k})$ is normalization constant to be specified later on in the text.

Similar to Eq. (2), the mode shape of the incoming wave could be expanded into vector spherical harmonics:

$$\mathbf{E}^{(\text{inc})}(\mathbf{r}) = \sum_{j=-\infty}^{\infty} e^{iajk_z} \sum_{l=m^*}^{\infty} [c_l^m \mathbf{M}_l^m(\mathbf{r}_j) + d_l^m \mathbf{N}_l^m(\mathbf{r}_j)],$$

$$\mathbf{H}^{(\text{inc})}(\mathbf{r}) = -i\sqrt{\epsilon} \sum_{j=-\infty}^{\infty} e^{iajk_z} \sum_{l=m^*}^{\infty} [c_l^m \mathbf{N}_l^m(\mathbf{r}_j) + d_l^m \mathbf{M}_l^m(\mathbf{r}_j)]. \tag{8}$$

According to [43], the expansion coefficient of the TE-polarized incident wave can be written as

$$c_l^m = \frac{i^m k_0}{\sqrt{C(\mathbf{k})} k_\perp} F_{l,m} \pi_{l,m}(\theta),$$

$$d_l^m = \frac{-i^m k_0}{\sqrt{C(\mathbf{k})} k_\perp} F_{l,m} \tau_{l,m}(\theta), \tag{9}$$

where θ is the angle between the wave vector $\mathbf{k}$ and the array axis z, $\cos(\theta) = k_z/k_0$:

$$\pi_{l,m}(\theta) = -\frac{\partial}{\partial\theta}P_l^m[\cos(\theta)],$$
$$\tau_{l,m}(\theta) = \frac{m}{\sin(\theta)}P_l^m[\cos(\theta)], \quad (10)$$

with P_l^m as the associated Legendre polynomials, and

$$F_{l,m} = (-1)^m i^l\sqrt{\frac{4\pi(2l+1)(l-m)!}{(l+m)!}}. \quad (11)$$

At the same time for the TM-polarized waves, we have

$$c_l^m = \frac{i^{m+1}k_0}{\sqrt{C(\mathbf{k})}k_\perp}F_{l,m}\tau_{l,m}(\theta),$$
$$d_l^m = -\frac{i^{m+1}k_0}{\sqrt{C(\mathbf{k})}k_\perp}F_{l,m}\pi_{l,m}(\theta). \quad (12)$$

For further analysis, we will use the quasi-modal expansion [35] based on the biorthogonal basis of the left $\mathbf{y}_n$ and right $\mathbf{x}_n$ eigenvectors of matrix $\widehat{\mathcal{L}}$:

$$\widehat{\mathcal{L}}\mathbf{x}_n = \lambda_n\mathbf{x}_n, \qquad \widehat{\mathcal{L}}^\dagger\mathbf{y}_n = \lambda_n^*\mathbf{y}_n. \quad (13)$$

It should be noted that $\widehat{\mathcal{L}}$ and, consequently, $\lambda_s, \mathbf{x}_s, \mathbf{y}_s$ are dependent on both β and k_0 [23]. The biorthogonal eigenvectors obey the following normalization condition:

$$\mathbf{y}_n^\dagger\mathbf{x}_{n'} = \mathbf{x}_n^\dagger\mathbf{y}_{n'} = \delta_{n,n'}. \quad (14)$$

For further convenience, the right eigenvector can be explicitly written as a vector of expansion coefficients over spherical harmonics in Eq. (2):

$$\mathbf{y} = \{a_l^m, b_l^m\}, \quad (15)$$

where, for simplicity, we omitted subscript n. Substituting the coefficients a_l^m, b_l^m to Eq. (2) instead of $\overline{a}_l^m, \overline{b}_l^m$ one can produce the profile of the optical quasi-mode.

Taking into account Eqs. (13) and (14), the inverse of $\widehat{\mathcal{L}}$ is given by

$$\widehat{\mathcal{L}}^{-1} = \sum_n\frac{1}{\lambda_n}\mathbf{x}_n\mathbf{y}_n^\dagger. \quad (16)$$

Applying Eq. (16), we can write the solution of the scattering problem in Eq. (3) under illumination by the incident wave in Eq. (6) in the following form:

$$\mathbf{p}^{(p)} = \sum_n\frac{w_n^{(p)}}{\lambda_n}\mathbf{x}_n, \quad (17)$$

with

$$w_n^{(p)} = \mathbf{y}_n^\dagger\mathbf{q}^{(p)}, \quad (18)$$

where $p = e, h$ is used for TM or TE waves, respectively. The entries of vector $\mathbf{q}^{(p)} = \{c_l^m, d_l^m\}$ are defined by Eqs. (9) and (12) depending on polarization. Further on, the quantity w_n introduced in Eq. (18) will be referred to as the *quasi-mode coupling strength*. The quasi-mode coupling strength can be expressed through expansion coefficients a_l^m, b_l^m as

$$w^{(h)} = \frac{i^m k_0}{\sqrt{C(\mathbf{k})}k_\perp}\sum_l F_{l,m}[\pi_{l,m}(a_l^m)^* - \tau_{l,m}(b_l^m)^*],$$
$$w^{(e)} = \frac{i^{m+1}k_0}{\sqrt{C(\mathbf{k})}k_\perp}\sum_l F_{l,m}[\tau_{l,m}(a_l^m)^* - \pi_{l,m}(b_l^m)^*], \quad (19)$$

where we again omitted subscript n for simplicity.

3. BOUND STATES IN THE CONTINUUM

The linear arrays of dielectric spheres possess rotational symmetry about the axis of periodicity and, thus, preserve the orbital angular momentum (OAM) of light. As a consequence, the system supports BICs with quantized OAM, including twisted BICs with nonzero OAM [44,45]. For simplicity and brevity of presentation in this paper, we restrict ourselves with the case of zero OAM $m = 0$ [23]. We shall also remain in the domain where only the zeroth diffraction order is allowed in the far-field radiation:

$$k_z a < k_0 d < 2\pi - k_z a. \quad (20)$$

This allows us to equate the Bloch wavenumber with the z-component of the incident wave vector, $k_z = \beta$. Under condition in Eq. (20), the system supports only two far-field scattering channels, one TM- and one TE-polarized. BICs are source-free solutions of Eq. (3) that exist even without the array being illuminated from the far zone to yield a simple condition:

$$\det[\widehat{\mathcal{L}}(k_0, \beta)] = 0. \quad (21)$$

The above condition means that, in the BIC-point, there is an eigenvector $\mathbf{y}_0$ with zero eigenvalue:

$$\widehat{\mathcal{L}}^\dagger\mathbf{y}_0 = 0, \quad (22)$$

which obviously corresponds to the BIC mode shape. Technically, the BICs can be found by searching for the zeros of $\det[\widehat{\mathcal{L}}(k_0, \beta)]$ in k_0, β-space. It is, however, more numerically efficient to only find the eigenvalue of $\widehat{\mathcal{L}}$ with the least absolute value. With respect to β, the BICs can be split into two classes [23], in-Γ standing wave BICs with $\beta = 0$ and off-Γ travelling wave (Bloch) BICs with $\beta \neq 0$. In this paper, we shall be concerned with in-Γ BICs, although the application of the proposed theory to off-Γ BICs is straightforward.

As mentioned in the introduction, the BICs are an exceptional point of the leaky zone in which the Q-factor diverges to infinity. Each leaky zone is characterized by dispersion of the complex eigenfrequency

$$\Omega = \omega_0 - i\gamma, \quad (23)$$

where ω_0 and γ are the position and the width of the resonance, respectively. The Q-factor is defined as

$$Q = \frac{\omega_0}{2\gamma}, \quad (24)$$

with γ obviously vanishing in the point of a BIC. The complex eigenfrequencies can be found by analytic extension of Eq. (21) to the complex plane as a function of k_0. In Fig. 2, we show results of numerical simulations for both TE- and TM-polarized waves with $m = 0$. Importantly, in the case $m = 0$, the waves of TE- and TM-polarizations are not coupled by matrix $\widehat{\mathcal{L}}$ [23]. Thus, all waves are pure TE- or TM-polarized, and only a single decay channel is allowed for each polarization. In Figs. 2(a) and 2(b), we show the mode profiles of TE BICs. Note that, in Fig. 2(a), H_z is antisymmetric with respect to the axis of the array. That is an example of so-called symmetry-protected BICs, which are symmetrically mismatched with the TE scattering channel. In contrast with the previous case, the BIC from Fig. 2(b) is not symmetry protected. The mode profile of a TM symmetry-protected BIC is shown in Fig. 2(c).

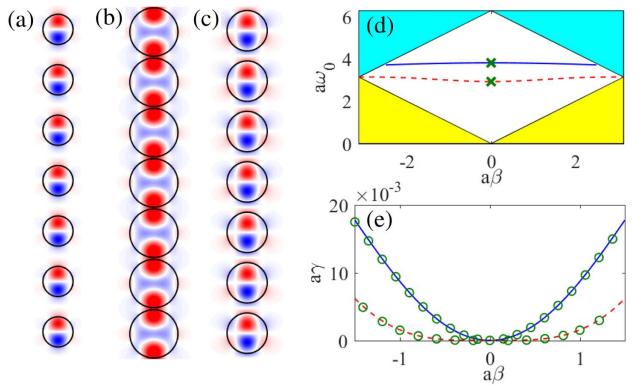

Fig. 2. BICs in the dielectric array from Fig. 1 with $\epsilon = 15$. (a) The z component of magnetic field, H_z for the symmetry-protected TE BIC with $ak_0 = 3.8141$ and $R = 0.3000a$. (b) H_z for the nonsymmetry-protected TE BIC with $ak_0 = 2.9375$ and $R = 0.480079a$. (c) The z component of electric field, E_z, for symmetry-protected TM BIC with $ak_0 = 3.6021$ and $R = 0.4000a$. (d) Dispersion of the real part of the eigenfrequency, ω_0, for the TE leaky modes hosting the BICs; solid blue indicates the leaky mode with a symmetry-protected BIC; dashed red indicates the leaky mode hosting the nonsymmetry-protected BIC. The white area is the domain where two scattering channels are open [Eq. (20)]. The positions of the in-Γ BICs are marked by crosses. (e) Dispersion of the imaginary part of the eigenfrequency, γ, for the TE leaky modes in the vicinity of the Γ-point; solid blue indicates the leaky mode with the symmetry-protected BIC; dashed red indicates leaky mode with the nonsymmetry-protected BIC. Green circles show the results obtained with Eq. (50).

In Figs. 2(d) and 2(e), we show the dispersion of ω_0 and γ, respectively, for TE leaky modes. Note that, on approach to the Γ-point for the nonsymmetry protected BIC, γ vanishes faster than for the symmetry-protected ones. As found in [46], this reflects in different asymptotics of the Q-factor for symmetry-protected and nonsymmetry-protected BICs at the Γ-point, the difference to be explained in Section 5.

4. COUPLED MODE THEORY

To understand the features of the resonant response in the spectral vicinity of a BIC in infinite arrays, we resort to coupled mode theory (CMT) [39,40]. CMT is a rather generic phenomenological approach relying on the modal representation of the EM field in the scattering domain. Each mode is viewed as an environment coupled oscillator with complex eigenfrequency [Eq. (23)]. One condition essential for CMT is the energy conservation. To account for the energy conservation, the system's modes must be energy normalized. Moreover, the mode shapes of the scattering channels must be normalized to supply (retrieve) a unit energy flux into (from) the scattering domain. To explicitly define the channels, we consider the total EM field far from the scattering domain. Following [47], we decompose the far field into incoming and outgoing waves:

$$E_z^{(\mathrm{tot})}(H_z^{(\mathrm{tot})}) = \frac{e^{im\phi+ik_z z}}{\sqrt{C(\mathbf{k})}}[a_{e,(h)}^{(+)}H_m^{(2)}(k_\perp\rho) + a_{e,(h)}^{(-)}H_m^{(1)}(k_\perp\rho)], \tag{25}$$

where $H_m^{(1,2)}(x)$ are the Hankel functions, $a_{e,h}^{(+)}$ is the amplitude of the incoming wave, and $a_{e,h}^{(-)}$ is the amplitude of the outgoing wave. The vectors of the incoming $\mathbf{a}^{(+)} = \{a_e^{(+)}, a_h^{(+)}\}$ and the outgoing $\mathbf{a}^{(-)} = \{a_e^{(-)}, a_h^{(-)}\}$ amplitudes are linked through the $\hat{\mathcal{S}}$-matrix

$$\mathbf{a}^{(-)} = \widehat{\mathcal{S}}\mathbf{a}^{(+)}. \tag{26}$$

The $\hat{\mathcal{S}}$-matrix defined in Eq. (26) has the following property:

$$\widehat{\mathcal{S}}^T = \widehat{\sigma}_z\widehat{\mathcal{S}}\widehat{\sigma}_z, \tag{27}$$

where $\widehat{\sigma}_z$ is the third Pauli matrix. Equation (27) can be easily proved using $\hat{\mathcal{S}}$-matrix unitarity, taking into account that that the magnetic field is a quasi-vector, which flips its sign under the time-reversal operation. At this point, we remind the reader that, for $m = 0$, the polarization conversion is forbidden and, hence, $\widehat{\mathcal{S}}$ is diagonal. On the other hand, because the incident wave in Eq. (6) is defined through the Bessel rather than the Hankel functions, we can write

$$E_z^{(\mathrm{tot})}(H_z^{(\mathrm{tot})}) = \frac{e^{im\phi+ik_z z}}{\sqrt{C(\mathbf{k})}}[a_{e,(h)}^{(+)}2J_m(k_\perp\rho) + a_{e,(h)}H_m^{(1)}(k_\perp\rho)], \tag{28}$$

where $a_{e,h}$ are unknown coefficients to be found by solving the scattering problem. The far-field solution can be expressed through matrix $\widehat{\mathcal{T}}$ as

$$\mathbf{a} = \widehat{\mathcal{T}}\mathbf{a}^{(+)}, \tag{29}$$

where $\mathbf{a} = \{a_e, a_h\}$. For the further convenience, we designate the elements of $\widehat{\mathcal{T}}$ as follows:

$$\widehat{\mathcal{T}} = \begin{Bmatrix} t_{e,e} & 0 \\ 0 & t_{h,h} \end{Bmatrix}. \tag{30}$$

Following [47], with the use of the identity $2J_m(x) = H_m^{(1)}(x) + H_m^{(2)}(x)$, one finds from Eqs. (25) and (28) that

$$\widehat{\mathcal{T}} = \widehat{\mathcal{S}} - \widehat{\mathbb{I}}. \tag{31}$$

Notice that, unlike $\widehat{\mathcal{S}}$, matrix $\widehat{\mathcal{T}}$ is generally nonunitary.

The goal of this paper is to construct a CMT for matrix $\widehat{\mathcal{S}}$. The mode shape of the TM- (TE) scattering channel is implicitly defined by Eq. (25) as

$$E_z^{(\mathrm{inc,out})}(H_z^{(\mathrm{inc,out})}) = \frac{1}{\sqrt{C(\mathbf{k})}}H_m^{(1,2)}(k_\perp\rho)e^{im\phi+ik_z z}, \tag{32}$$

where (inc, out) stand for the incoming wave and outgoing wave, respectively. By requiring that each scattering channel supplies a unit energy flux per period of the array, we can find the normalization constant in Eq. (32) as

$$C(\mathbf{k}) = \frac{2k_0}{k_\perp^2}. \tag{33}$$

Technically, the above result is obtained by finding the total Poynting of the channel function in Eq. (32) through the cylindrical surface enveloping the elementary cell of the array. Under the above condition, the response of a *single* resonant mode to impinging waves is described by the following equations [47]:

$$b = \frac{\boldsymbol{\kappa}^T\mathbf{a}^{(+)}}{i(\omega_0 - \omega) + \gamma}, \tag{34}$$

$$\mathbf{a}^{(-)} = \widehat{\mathcal{C}}\mathbf{a}^{(+)} + b\mathbf{d}, \tag{35}$$

where b is the amplitude of the resonant mode, $\widehat{\mathcal{C}}$ is the scattering matrix of direct (nonresonant) transmission path, and vectors $\boldsymbol{\kappa}, \mathbf{d}$ describe the coupling between the resonant mode and the incoming and outgoing waves, respectively. Most importantly, the quantities γ, $\mathbf{d}$, and $\widehat{\mathcal{C}}$ introduced in Eqs. (34) and (35) are not independent. The relationships among γ, $\mathbf{d}$, and $\widehat{\mathcal{C}}$ can be established by performing the time-reversal operation [39,40,47]. To apply the time-reversal arguments, one has to take into account that, under the time reversal, the channel functions in Eq. (32) change the sign of both β and m. This has been rigorously done in [47,48]. In our case, however, the system possesses both rotational symmetry and symmetry with respect to the mirror reflection in the x_0y–plane. Thus, we can conclude that γ, $\mathbf{d}$, and $\widehat{\mathcal{C}}$ are immune to the time reversal. Then, following the standard procedure from [39], one finds

$$\widehat{\mathcal{C}}\widehat{\sigma}_z\mathbf{d}^* = -\mathbf{d}, \tag{36}$$

$$\mathbf{d}^\dagger\mathbf{d} = 2\gamma, \tag{37}$$

$$\kappa = \widehat{\sigma}_z\mathbf{d}. \tag{38}$$

Note that the above expression only differs from the standard two-channel CMT [39] by emergence of $\hat{\sigma}_z$, which simply reflects the behavior of the channel functions in Eq. (32) under the time reversal. The final expression for the scattering matrix reads

$$\widehat{\mathcal{S}} = \widehat{\mathcal{C}} + \frac{\mathbf{d}\mathbf{d}^T}{i(\omega_0 - \omega) + \gamma}\widehat{\sigma}_z. \tag{39}$$

Now using Eqs. (31) and (39), one can write the solution under illumination by the Bessel waves:

$$\mathbf{a} = \left(-\mathbb{I} + \widehat{\mathcal{C}} + \frac{\mathbf{d}\mathbf{d}^T}{i(\omega_0 - \omega) + \gamma}\widehat{\sigma}_z\right)\mathbf{a}^{(+)}. \tag{40}$$

To establish a link between Eq. (17) and the CMT solution in Eq. (40), we consider the resonant contribution to Eq. (17), i.e., the singular term with vanishing λ_n in the denominator. In what follows, we omit the subscript n, keeping in mind that only the resonant contribution is considered. The resonant term reads

$$\mathbf{f} = \frac{\mathbf{w}^T\mathbf{a}^{(+)}}{\lambda}\mathbf{x}, \tag{41}$$

where $\mathbf{w} = \{w^{(e)}, w^{(h)}\}$. Let us now write a series expansion in ω in the vicinity of the leaky mode resonant eigenfrequency ω_0 with a fixed β near the normal incidence:

$$\begin{aligned}\mathbf{w} &= \mathbf{w}_0 + \mathbf{w}_1(\omega - \omega_0),\\ \lambda &= \lambda_0 + \lambda_1(\omega - \omega_0),\\ \mathbf{x} &= \mathbf{x}_0 + \mathbf{x}_1(\omega - \omega_0),\end{aligned} \tag{42}$$

where

$$\mathbf{w}_{0,1} = \{w_{0,1}^{(e)}, w_{0,1}^{(h)}\}. \tag{43}$$

Note that all quantities introduced in Eq. (42) are dependent on β. Expanding Eq. (41) up to the first order in $\omega - \omega_0$, we have

$$\mathbf{f} = (\mathbf{g}_0^T\mathbf{a}^{(+)})\mathbf{x}_0 + (\mathbf{g}_1^T\mathbf{a}^{(+)})\mathbf{x}_1, \tag{44}$$

with

$$\mathbf{g}_0 = \frac{\left(\mathbf{w}_0 - \frac{\lambda_0}{\lambda_1}\mathbf{w}_1\right)}{\lambda_0 + \lambda_1(\omega - \omega_0)} + \frac{1}{\lambda_1}\mathbf{w}_1, \tag{45}$$

$$\mathbf{g}_1 = \frac{-\frac{\lambda_0}{\lambda_1}\mathbf{w}_0}{\lambda_0 + \lambda_1(\omega - \omega_0)} + \frac{1}{\lambda_1}\mathbf{w}_0. \tag{46}$$

Before comparing Eq. (44) against Eq. (34), we have to renormalize the resonant mode to support a unit energy per period of the array,

$$\overline{\mathbf{x}}_0 = \mathbf{x}_0/\sqrt{C_0}, \tag{47}$$

where C_0 is the normalization constant. Because the optical quasi-mode $\overline{\mathbf{x}}_0$ is unit-normalized, the outgoing field can be produced with the CMT coupling vector $\mathbf{d}$:

$$\mathbf{a} = \sqrt{C_0}(\mathbf{d}\mathbf{g}_0^T)\mathbf{a}^{(+)}. \tag{48}$$

Equating the resonant term in Eq. (40) to that in Eq. (48), we obtain the following equations:

$$\begin{aligned}-i\sqrt{C_0}\left(\mathbf{w}_0 - \frac{\lambda_0}{\lambda_1}\mathbf{w}_1\right) &= \lambda_1\widehat{\sigma}_z\mathbf{d},\\ \sqrt{C_0}\gamma\left(\mathbf{w}_0 - \frac{\lambda_0}{\lambda_1}\mathbf{w}_1\right) &= \lambda_0\widehat{\sigma}_z\mathbf{d}.\end{aligned} \tag{49}$$

One can immediately see from the above equations that

$$\gamma = -i\frac{\lambda_0}{\lambda_1}. \tag{50}$$

The coefficient λ_1 is a nonvanishing quantity; hence, λ_0 and γ exhibit the same asymptotics in the vicinity of the BIC. Note that the resonant term in Eq. (46) can be dropped because it vanishes with λ_0. Equation (50) can be used for finding the resonant width of the high-Q leaky zone without the use of analytic extension to the complex plane. One can see from Fig. 2(e) that Eq. (50) demonstrates good agreement with the true resonant width found from the analytic extension in the vicinity of the Γ-point. For example, if $a\beta = 0.5$ for the leaky mode with the symmetry protected BIC, we have $a\Omega = 3.80950 - i0.00231$, while the analytic extension yields $a\Omega = 3.80947 - i0.002299$. Remarkably, by definition [Eq. (42)], it is not guaranteed that γ found from Eq. (50) is a real positive quantity. It appears to be a challenging task to prove that Eq. (50) is generally real positive. Our numerical results, however, indicate that it is always real positive in consistence with definition Eq. (23). Moreover, it is found that λ_0 is always real negative, while λ_1 is imaginary positive. In Fig. 3(a), we show the dependence of λ on ω in the spectral vicinity of the symmetry protected BIC from Fig. 2(a). Next, we further analyze Eq. (49) depending on the polarization of the scattering channels for $m = 0$.

A. TE Modes

Using Eq. (37), vector $\mathbf{d}$ for TE modes can be written as

$$\mathbf{d} = \begin{Bmatrix} 0 \\ \gamma_h \end{Bmatrix}, \qquad 2\gamma = |\gamma_h|^2. \tag{51}$$

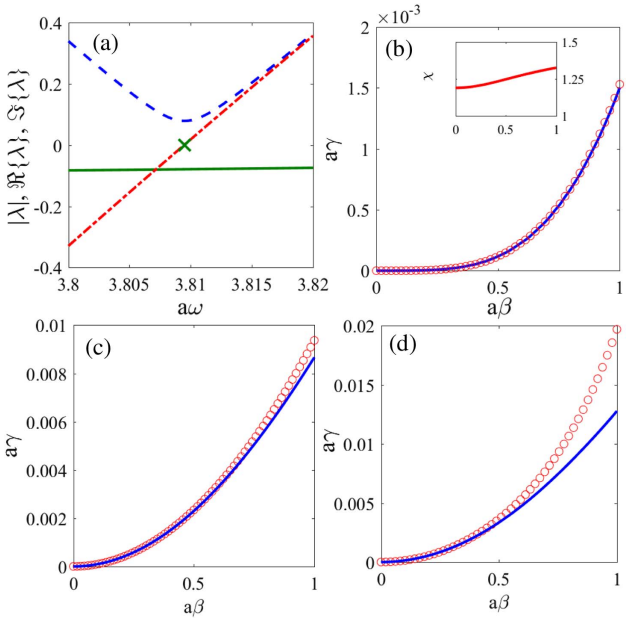

Fig. 3. (a) Resonant eigenvalue λ in the spectral vicinity $a\beta = 0.5$ of the symmetry protected BIC from Fig. 2(a); dashed blue line indicates $|\lambda|$; solid green line indicates $\Re\{\lambda\}$; dashed–dotted red line indicates $\Im\{\lambda\}$; the position of the resonance is shown by a green cross. (b) Resonant width γ found from Eq. (50) for the leaky zone with the nonsymmetry-protected BIC 2 (b) indicated by a solid blue line, and as $\gamma = |\gamma_b|^2/2$ from Eq. (55). Inset shows the dependence of the phase of the CMT coupling coefficient χ on β. (c), (d) The same as in (b) for TE and TM symmetry-protected BIC from Figs. 2(a) and 2(c), respectively.

One can see from Eqs. (50) and (51) that λ_0 vanishes faster, then γ_b, and we can drop the second term in the round brackets in Eq. (49). For the CMT coupling coefficient, we have

$$\gamma_b = i\frac{\sqrt{C_0}}{\lambda_1} w_0^{(b)}, \tag{52}$$

which dictates the same asymptotic behavior of γ_b and $w_b^{(0)}$. By applying Eq. (38), we also have

$$C_0 = 2\gamma \left| \frac{\lambda_1}{w_0^{(b)}} \right|^2. \tag{53}$$

Thus, we can express all features of the resonant response through only three parameters λ_0, λ_1, and w_0. Taking into account the λ_1 is real positive, we can write

$$\gamma_b = \sqrt{2\gamma}\ \arg(w_0^{(b)}). \tag{54}$$

Unfortunately, Eq. (54) cannot be unambiguously applied for finding γ_b because the biorthogonal eigenvectors in Eq. (14) and, consequently, the quasi-mode coupling strength $w^{(b)}$ are defined up to an arbitrary phase factor. To avoid the problem with the arbitrary phase factor, we apply an alternative approach for calculating γ_b based on finding the far-field structure of quasi-mode $\mathbf{x}$. Details of the approach are described in Appendix A. The final result reads

$$\gamma_b = \frac{\pm k_\perp}{2} \sqrt{\frac{1}{|\lambda_1| a k_0^3}} \overline{w}_0^{(b)}. \tag{55}$$

Note that Eq. (55) allows us to determine γ_b up to its sign. This, however, does not affect the reflection coefficient defined by Eq. (40). In Figs. 3(b) and 3(c), we show the resonant width $\gamma = |\gamma_b|^2/2$ found from Eq. (55) for the leaky zones with the nonsymmetry-protected and symmetry-protected TE BICs, respectively, in comparison against Eq. (50) to demonstrate the agreement between the two approaches in the vicinity of the Γ-point. At large $|\beta|$, however, γ found from Eq. (55) deviates from the true resonant width. That imposes a limit on the CMT approach.

Because the polarization conversion is forbidden for $m = 0$, the scattered EM field is described by a single entry $t_{b,b}$ of matrix $\widehat{\mathcal{T}}$, Eq. (30). The only relevant element of the scattering matrix of the direct process can be found from Eq. (36) as

$$\{\widehat{C}\}_{b,b} = \gamma_b^2/|\gamma_b|^2. \tag{56}$$

By using Eq. (40), the final solution for $t_{b,b}$ can be written as

$$t_{b,b} = -1 - e^{i2\chi} \frac{\omega - \omega_0 - i\gamma}{\omega - \omega_0 + i\gamma}, \tag{57}$$

where χ is the phase of the CMT coupling coefficient γ_b, $\chi = \arg(\gamma_b)$. The dependence of χ on β is shown in the inset to Fig. 3(b). In Figs. 4(a) and 4(b), we show the CMT spectrum Eq. (57) of the reflection coefficient $t_{b,b}$ near the Γ-point for the leaky zone with the symmetry-protected BIC in Fig. 1(a) in comparison with the exact numerical solution obtained from Eq. (3). Two values of β are chosen for numerical simulations to demonstrate that the accuracy of the CMT solution drops away off the Γ-point. However, one can see from Figs. 4(a) and 4(b) that, even at the distance of one-fourth of the Brillouin zone, the CMT approach is capable of reproducing the Fano feature in the reflection spectrum.

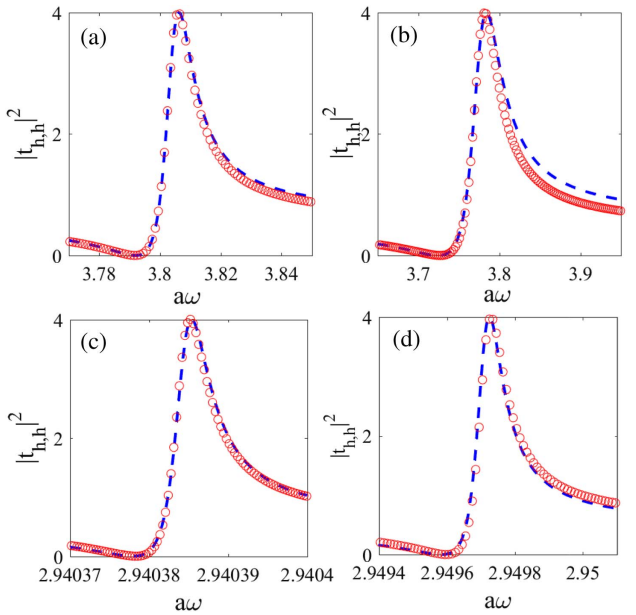

Fig. 4. Optical response induced by the TE BICs from Fig. 1. Blue dashed line indicates exact numerical solution by Eq. (3); red circles indicate CMT approximation. (a) Symmetry-protected BIC, $a\beta = 0.7424$; (b) symmetry-protected BIC, $a\beta = 1.5000$; (c) nonsymmetry-protected BIC, $a\beta = 0.1837$; (d) nonsymmetry-protected BIC, $a\beta = 0.3878$.

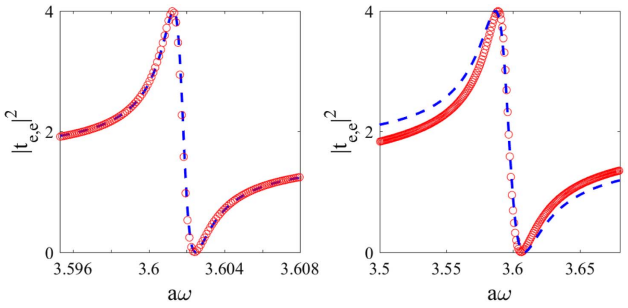

Fig. 5. Optical response induced by symmetry-protected TM BIC from Fig. 2(c). Blue dashed line indicates exact numerical solution by Eq. (3); red circles indicate CMT approximation. Left panel, $a\beta = 0.2041$; right panel, $a\beta = 0.7959$.

Similar simulations were undertaken for the nonsymmetry-protected BIC in Fig. 1(b). The results are shown in Figs. 4(a) and 4(b). Again, one can see good agreement between the CMT and exact solutions far off the Γ-point. Although, in the present case, the accuracy drops faster than for the symmetry-protected BIC.

B. TM Modes

CMT for TM modes can be easily constructed along the same line as in the previous subsection. For vector **d**, we have

$$\mathbf{d} = \begin{Bmatrix} \gamma_e \\ 0 \end{Bmatrix}, \qquad 2\gamma = |\gamma_e|^2, \tag{58}$$

while the coupling coefficient is found as (see Appendix A)

$$\gamma_e = \frac{\pm k_\perp}{2}\sqrt{\frac{1}{|\lambda_1| a k_0^3}}\overline{w}_0^{(e)}. \tag{59}$$

The relevant entry of the scattering matrix of the direct process reads

$$\widehat{\mathcal{C}}_{e,e} = -\gamma_e^2/|\gamma_e|^2. \tag{60}$$

In Fig. 3(d), we plot the resonant width found from Eq. (60) in comparison against Eq. (50) to demonstrate that the two approaches converge at the Γ-point. The spectrum of the reflection coefficient $t_{e,e}$ for a symmetry-protected TM BIC from Fig. 2(c) is shown in Fig. 5 in comparison with the CMT predictions. As before, we see good agreement between the CMT and exact numerical solutions.

5. ASYMPTOTIC BEHAVIOR OF THE CMT COUPLING COEFFICIENTS

The expansion coefficients a_l^m, b_l^m for any quasi-mode have the following property as functions of the Bloch wavenumber β:

$$\begin{aligned} a_l^m(-\beta) &= (-1)^{l+s} a_l^m(\beta), \\ b_l^m(-\beta) &= (-1)^{l+1+s} b_l^m(\beta), \end{aligned} \tag{61}$$

where $s = 0, 1$. This property reflects the symmetry of the system defined by simultaneous change of the sign of β and mirror reflection in the plane perpendicular to the array axis z. In this section, we consider the asymptotic behavior of the CMT coefficients against β in the spectral vicinity of a BIC, i.e., at near normal incidence, having in mind Eq. (61).

A. Symmetry-Protected BIC with $m = 0$

Such in-Γ BICs can be either TE- or TM-polarized. Here, we consider TE-polarized standing wave BIC. This BIC is hosted by a TE-polarized leaky zone with the corresponding left eigenvector written as

$$\mathbf{y} = \{a_l^0(\beta), 0\}. \tag{62}$$

As far as the solution is symmetrically mismatched with the TE scattering channel, we have $s = 0$ in Eq. (61). This means that all odd expansion coefficients are zero in the Γ-point [23], $a_{2k+1}^m(0) = 0$. Applying Eq. (19) and noting that $\tau_{n,0} = 0$ according to Eq. (10), we have

$$w^{(h)}(\beta) = \sum_k F_{2k}^0 \pi_{2k}^0(\theta) a_{2k}^0(\beta) + \sum_k F_{2k+1}^0 \pi_{2k+1}^0(\theta) a_{2k+1}^0(\beta) \tag{63}$$

$$w^{(e)}(\beta) = 0. \tag{64}$$

By recollecting that $\cos(\theta) = \beta/k_0$ and using Eq. (10), one can show that

$$\tau_{l,m}(-\beta) = (-1)^{l+m}\tau_{l,m}(\beta), \quad \pi_{l,m}(-\beta) = (-1)^{l+m+1}\pi_{l,m}(\beta). \tag{65}$$

Next, referring to Eq. (61) with $s = 0$, we immediately see that both summands in Eq. (63) are odd with β. Hence, the leading term expansion at the Γ-point is given by

$$w^{(h)}(\beta) \propto \beta. \tag{66}$$

Finally, according to Eqs. (51) and (52), the CMT coupling coefficient and resonant width have the following asymptotics:

$$\gamma_h \propto \beta, \qquad \Gamma \propto \beta^2. \tag{67}$$

It is worth mentioning that the same arguments lead to the identical results for the symmetry-protected TM modes. The dependance of the quasi-mode coupling strength against β is shown in Fig. 6 along with the best fit with a linear function.

B. Nonsymmetry-Protected BIC with $m = 0$

In that case, the TE-polarized standing wave BIC is hosted by the leaky zone with $s = 1$ in Eq. (61), and now all even

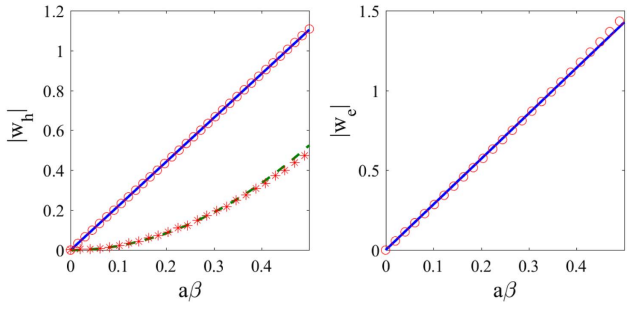

Fig. 6. Left panel: Quasi-mode coupling strength w_h for the TE leaky modes from Fig. 2(d). Red circles indicate the mode with asymmetry-protected BIC; red stars indicate the mode with a nonsymmetry-protected BIC. Solid blue and dashed green line show the best fit with linear and parabolic functions, respectively. Right panel: Red circles show the quasi-mode coupling strength w_e for the leaky mode with symmetry-protected TM BIC from Fig. 2(c). The solid blue line is the best fit with a linear function.

expansion coefficients are zero in the Γ-point [23], $a^m_{2k}(\beta)=0$. Consequently, both summands in Eq. (63) are even with β. In general, at the Γ-point, we have

$$w^{(h)}(\beta)\propto \text{Const}+\beta^2, \tag{68}$$

$$w^{(e)}(\beta)=0. \tag{69}$$

Note that $w^{(h)}(0)$ may be a nonvanishing quantity, and the leaky zone does not necessarily have a BIC in the Γ-point, which explains the difficulty in finding nonsymmetry-protected BICs in contrast with symmetry-protected ones. That always requires tuning the material parameters of a system to eliminate the constant term in Eq. (68). However, such a BIC is the most appealing to be employed for enhancement of light–matter interaction due to higher-order asymptotics of the CMT parameters

$$\gamma_h\propto\beta^2,\qquad \Gamma\propto\beta^4. \tag{70}$$

In Fig. 6, we also show the asymptotic behavior of w_e in the vicinity of the Γ-point, which is well fit to a parabola.

6. CONCLUSION

We considered the optical response induced by bound states in the continuum in arrays of dielectric spheres. By combining a quasi-mode expansion technique with coupled mode theory (CMT), we put forward a theory of the optical response by high-Q resonance surrounding BICs in momentum space. The central results are analytical expressions for the CMT parameters, which can be easily calculated from the eigenfrequencies and eigenvectors of the interaction matrix of the scattering systems. Once the CMT coupling coefficients are known, the optical response can be easily calculated through simple formulas. The results obtained are verified in comparison against exact numerical solutions to demonstrate that the CMT approximation is capable of reproducing Fano features in the spectral vicinity of the BIC. We expect that the proposed approach is not limited to arrays of a dielectric sphere. The complicated machinery related to cylindrical and spherical wave expansions is necessitated by our choice of the computational method. However, if the scattering problem is cast in the form of a set of linear equations similar to Eq. (3) by means of, say, finite difference or finite element methods, the quasi-mode expansion technique becomes equally applicable for any periodic structure supporting bound states in the continuum. Thus, we speculate that our results may be useful for engineering the resonant response in systems with diverging Q-factors.

Thus far, the asymptotic behavior of the critical light enhancement induced by BICs has been rigorously studied only in perforated slabs [3] and arrays of dielectric rods [31,32]. In this paper, we focus on linear arrays of dielectric spheres. Based on the quasi-mode expansion technique, we derived the asymptotic scaling law for the CMT parameters in the vicinity of the Γ-point. It is rigorously demonstrated that the linewidth in the CMT approximation exhibits different asymptotic behavior depending on the symmetry of the BIC. In particular, it is proved that, for symmetry-protected BIC, the Q-factor diverges as β^2 in the vicinity of the Γ-point. At the same time, for the BICs unprotected by symmetry, the Q-factor diverges as β^4. This suggests application of the nonsymmetry-protected BICs to achieve a stronger resonant effect for enhancement of light–matter interaction. We mention in passing that our findings totally comply with earlier observations [31,32,49].

In this paper, the analysis was limited to the case of zero angular momentum, i.e., to the situation when the waves of TE- and TM-polarization are decoupled. It would be interesting, though, to extend the results to the BIC with nonzero OAM [45], in which case the leaky mode is hybridized, and matrix $\widehat{\mathcal{T}}$ is no longer diagonal. This brings up certain difficulties in constructing CMT because the matrix of the direct process is no longer uniquely defined by the quasi-mode coupling strengths. Moreover, an extra difficulty arises in defining the phase of the CMT coupling constant because Eq. (85) is not applicable in subspaces with nonzero orbital angular momentum. The first principle derivation of CMT from the quasi-modal expansion for waves with nonzero OAM is our goal for future studies.

APPENDIX A

The solution for EM field for TE-quasi mode $\mathbf{x}$ with $m=0$ can be written as

$$\mathbf{E}=\sum_j e^{ijq\beta}\sum_{l=m^*}^{\infty}\tilde{a}^0_l\mathbf{M}^0_l(\mathbf{r}_j), \tag{A1}$$

where $\tilde{a}^0_l$ are the expansion coefficients for the right eigenvector $\mathbf{x}$:

$$\mathbf{x}=\{\tilde{a}^0_l\}. \tag{A2}$$

On the other hand, spherical vector harmonics $\mathbf{M}^0_l(\mathbf{r}_j)$ can be expressed through a scalar function $\psi^0_l(\mathbf{r}_j)$ as [50]

$$\mathbf{M}^0_l(\mathbf{r}_j)=\nabla\times[\mathbf{r}_j\psi^0_l(\mathbf{r}_j)], \tag{A3}$$

where

$$\psi^0_l(\mathbf{r}_j)=\frac{1}{\sqrt{l(l+1)}}h^{(1)}_l(k_0\mathbf{r}_j)Y^0_l(\theta,\phi), \tag{A4}$$

with $h^{(1)}_l(x)$ as the spherical Hankel function, and

$$Y^m_l(\theta,\phi)=(-1)^m\sqrt{\frac{(2l+1)(l-m)!}{4\pi(l+m)!}}e^{im\phi}P^m_l[\cos(\theta)]. \tag{A5}$$

Combining Eqs. (A1) and (A3) for the azimuthal component of the electric field $E_\phi(\mathbf{r})$, we have

$$E_\phi(\mathbf{r})=-e^{-i\phi}\sum_j e^{ijq\beta}\sum_{l=1}^{\infty}\tilde{a}^0_l h^{(1)}_l(k_0\mathbf{r}_j)Y^1_l(\theta,\phi), \tag{A6}$$

where we used

$$\frac{\partial P^0_l[\cos(\theta)]}{\partial\theta}=-P^1_l[\cos(\theta)]. \tag{A7}$$

According to [51], the series in Eq. (A6) can be rewritten as an expansion into cylindrical functions,

$$E_\phi(\mathbf{r})=-\sum_{n=-\infty}^{\infty}M_n e^{i\beta_n z}K_1\left(k_0\rho\sqrt{\left(\frac{\beta_n}{k_0}\right)^2-1}\right), \tag{A8}$$

where $K_1(x)$ is a modified Bessel function

$$\beta_n = \beta + \frac{2\pi}{a} n, \tag{A9}$$

and

$$M_n = \frac{2i}{k_0 a} \sum_{l=1}^{\infty} i^{-l} \tilde{a}_l^0 \sqrt{\frac{(2l+1)}{4\pi l(l+1)}} P_l^1\left(\frac{\beta_n}{k_0}\right). \tag{A10}$$

In the next step, we recall that, under condition Eq. (20), only the zeroth diffraction order $n = 0$ is present in the far-field radiation. In the far field, all waves can be written in the form of expansion into cylindrical functions. For such cylindrical waves, the electric $E_\phi(\mathbf{r})$ is linked to the axial component of the magnetic field $H_z(\mathbf{r})$ through the following equation:

$$E_\phi(\mathbf{r}) = -\frac{ik_0}{k_\perp^2} \frac{\partial H_z(\mathbf{r})}{\partial \rho}. \tag{A11}$$

By using

$$K_1(-ix) = -\frac{\pi}{2} H_1^{(1)}(x) \tag{A12}$$

and

$$H_1^{(1)}(x) = -\frac{\partial H_0^{(1)}(x)}{\partial x}, \tag{A13}$$

we obtain the far-zone EM field pattern generated by the optical quasi-mode:

$$H_z(\mathbf{r}) = -\frac{i\pi}{2} \frac{k_\perp}{k_0} M_0 e^{i\beta z} H_0^{(1)}(k_\perp \rho). \tag{A14}$$

The eigenvectors $\mathbf{y}$ and $\mathbf{x}$ are defined up to an arbitrary phase factor. Because the interaction matrix possesses the property $\{\hat{\mathcal{L}}\}_{l,l'} = (-1)^{l+l'} \{\hat{\mathcal{L}}\}_{l',l}$, one can show that vector $\overline{\mathbf{y}}$,

$$\{\overline{\mathbf{y}}\}_l = (-1)^l \{\mathbf{x}^*\}_l, \tag{A15}$$

is a left eigenvector of $\widehat{\mathcal{L}}$. In what follows, we set

$$\mathbf{y}_n = \overline{\mathbf{y}}_n, \tag{A16}$$

which allows us to eliminate the disambiquety of the phase definition [49]. Using the definition of the expansion coefficient for vector $\mathbf{q}$, in Eq. (9) we find

$$M_0 = \frac{2i\sqrt{C(\mathbf{k})} k_\perp}{k_0^2 a} \frac{1}{4\pi} \mathbf{q}^\dagger \mathbf{x}. \tag{A17}$$

Applying Eq. (A15) according to [49], one can show that $\mathbf{q}^\dagger \mathbf{x} = \mathbf{y}^\dagger \mathbf{q}$, which, together with Eq. (19), yields

$$M_0 = \frac{2i\sqrt{C(\mathbf{k})} k_\perp}{k_0^2 a} \frac{1}{4\pi} w^{(b)}. \tag{A18}$$

Physically, Eq. (A14) is the far-field pattern of the quasi-mode specified by vector $\mathbf{x}$; therefore, the far-field solution produced by the term Eq. (41) with vanishing λ in the denominator can be written as

$$H_z^{(\mathrm{out})}(\mathbf{r}) = \frac{k_\perp^2 \sqrt{C(\mathbf{k})}}{4ak_0^3} \frac{(w^{(b)})^2}{\lambda} H_0^{(1)}(k_\perp \rho) e^{i\beta z} a_b^{(+)}. \tag{A19}$$

Using the series expansion in Eq. (42), we find the resonant contribution into the outgoing far field radiation is

$$H_z^{(\mathrm{res})}(\mathbf{r}) = \frac{k_\perp^2 \sqrt{C(\mathbf{k})}}{i4\lambda_1 a k_0^3} \frac{(w_0^{(b)})^2}{i(\omega_0 - \omega) + \gamma} H_0^{(1)}(k_\perp \rho) e^{i\beta z} a_b^{(+)}. \tag{A20}$$

We mention in passing that the discrepancy seen in Figs. 3(c) and 3(d) is caused by approximation in the series expansion [Eq. (42)]. On the other hand, according to Eqs. (40) and (51), the CMT solution for the resonant term reads

$$H_z^{(\mathrm{res})}(\mathbf{r}) = -\gamma_b^2 \frac{1}{\sqrt{C(\mathbf{k})}} \frac{1}{i(\omega_0 - \omega) + \gamma} H_0^{(1)}(k_\perp \rho) e^{i\beta z} a_b^{(+)}. \tag{A21}$$

Comparing Eq. (A20) against Eq. (A21), we find

$$\gamma_b^2 = -\frac{k_\perp^2 C(\mathbf{k})}{i4\lambda_1 a k_0^3} (w_0^{(b)})^2. \tag{A22}$$

According to Eq. (19), the quantity $w_0^{(b)}$ is introduced with $\sqrt{C(\mathbf{k})}$ in the denominator. One can see that the final result is independent of $C(\mathbf{k})$, which can be removed from Eq. (A22). By using

$$\overline{w}_0^{(b)} = w_0^{(b)} \sqrt{C(\mathbf{k})}, \tag{A23}$$

that yields

$$\gamma_b^2 = -\frac{k_\perp^2}{i4\lambda_1 a k_0^3} (\overline{w}_0^{(b)})^2. \tag{A24}$$

Finally, by recollecting that λ_1 is imaginary positive for γ_b, we have Eq. (55). Essentially, the same derivation can be equally applied to the TM modes with $m = 0$ leading to Eq. (59) with

$$\overline{w}_0^{(e)} = w_0^{(e)} \sqrt{C(\mathbf{k})}. \tag{A25}$$

Funding. Ministry of Education and Science of the Russian Federation (Minobrnauka) (State Contract N 3.1845.2017); Russian Foundation for Basic Research (RFBR) (16-02-00314).

REFERENCES

1. S. John, "Why trap light?" Nat. Mater. **11**, 997–999 (2012).
2. C. W. Hsu, B. Zhen, A. D. Stone, J. D. Joannopoulos, and M. Soljačić, "Bound states in the continuum," Nat. Rev. Mater. **1**, 16048 (2016).
3. S. P. Shipman and S. Venakides, "Resonant transmission near non-robust periodic slab modes," Phys. Rev. E **71**, 026611 (2005).
4. J. M. Foley, S. M. Young, and J. D. Phillips, "Symmetry-protected mode coupling near normal incidence for narrow-band transmission filtering in a dielectric grating," Phys. Rev. B **89**, 165111 (2014).
5. J. M. Foley and J. D. Phillips, "Normal incidence narrowband transmission filtering capabilities using symmetry-protected modes of a subwavelength, dielectric grating," Opt. Lett. **40**, 2637–2640 (2015).
6. X. Cui, H. Tian, Y. Du, G. Shi, and Z. Zhou, "Normal incidence filters using symmetry-protected modes in dielectric subwavelength gratings," Sci. Rep. **6**, 36066 (2016).
7. C. Blanchard, J.-P. Hugonin, and C. Sauvan, "Fano resonances in photonic crystal slabs near optical bound states in the continuum," Phys. Rev. B **94**, 155303 (2016).
8. S. Hein, W. Koch, and L. Nannen, "Trapped modes and Fano resonances in two-dimensional acoustical duct-cavity systems," J. Fluid Mech. **692**, 257–287 (2012).
9. C. S. Kim, A. M. Satanin, Y. S. Joe, and R. M. Cosby, "Resonant tunneling in a quantum waveguide: effect of a finite-size attractive impurity," Phys. Rev. B **60**, 10962–10970 (1999).
10. V. Mocella and S. Romano, "Giant field enhancement in photonic resonant lattices," Phys. Rev. B **92**, 155117 (2015).

11. J. W. Yoon, S. H. Song, and R. Magnusson, "Critical field enhancement of asymptotic optical bound states in the continuum," Sci. Rep. **5**, 18301 (2015).
12. A. Kodigala, T. Lepetit, Q. Gu, B. Bahari, Y. Fainman, and B. Kanté, "Lasing action from photonic bound states in continuum," Nature **541**, 196–199 (2017).
13. B. Bahari, F. Vallini, T. Lepetit, R. Tellez-Limon, J. Park, A. Kodigala, Y. Fainman, and B. Kante, "Integrated and steerable vortex lasers," arXiv:1707.00181 (2018).
14. S. T. Ha, Y. H. Fu, N. K. Emani, Z. Pan, R. M. Bakker, R. Paniagua-Dominguez, and A. I. Kuznetsov, "Lasing action in active dielectric nanoantenna arrays," arXiv:1803.09993 (2018).
15. F. R. Ndangali and S. V. Shabanov, "The resonant nonlinear scattering theory with bound states in the radiation continuum and the second harmonic generation," Proc. SPIE **8808**, 88081F (2013).
16. T. Wang and S. Zhang, "Large enhancement of second harmonic generation from transition-metal dichalcogenide monolayer on grating near bound states in the continuum," Opt. Express **26**, 322–337 (2018).
17. S. Romano, A. Lamberti, M. Masullo, E. Penzo, S. Cabrini, I. Rendina, and V. Mocella, "Optical biosensors based on photonic crystals supporting bound states in the continuum," Materials **11**, 526 (2018).
18. S. Venakides and S. P. Shipman, "Resonance and bound states in photonic crystal slabs," SIAM J. Appl. Math. **64**, 322–342 (2003).
19. D. C. Marinica, A. G. Borisov, and S. V. Shabanov, "Bound states in the continuum in photonics," Phys. Rev. Lett. **100**, 183902 (2008).
20. C. W. Hsu, B. Zhen, J. Lee, S.-L. Chua, S. G. Johnson, J. D. Joannopoulos, and M. Soljačić, "Observation of trapped light within the radiation continuum," Nature **499**, 188–191 (2013).
21. F. Monticone and A. Alù, "Embedded photonic eigenvalues in 3D nanostructures," Phys. Rev. Lett. **112**, 213903 (2014).
22. Y. Yang, C. Peng, Y. Liang, Z. Li, and S. Noda, "Analytical perspective for bound states in the continuum in photonic crystal slabs," Phys. Rev. Lett. **113**, 037401 (2014).
23. E. N. Bulgakov and A. F. Sadreev, "Light trapping above the light cone in a one-dimensional array of dielectric spheres," Phys. Rev. A **92**, 023816 (2015).
24. L. Ni, Z. Wang, C. Peng, and Z. Li, "Tunable optical bound states in the continuum beyond in-plane symmetry protection," Phys. Rev. B **94**, 245148 (2016).
25. E. N. Bulgakov and D. N. Maksimov, "Light guiding above the light line in arrays of dielectric nanospheres," Opt. Lett. **41**, 3888 (2016).
26. Z. F. Sadrieva, I. S. Sinev, K. L. Koshelev, A. Samusev, I. V. Iorsh, O. Takayama, R. Malureanu, A. A. Bogdanov, and A. V. Lavrinenko, "Transition from optical bound states in the continuum to leaky resonances: role of substrate and roughness," ACS Photon. **4**, 723–727 (2017).
27. F. Monticone and A. Alù, "Bound states within the radiation continuum in diffraction gratings and the role of leaky modes," New J. Phys. **19**, 093011 (2017).
28. L. Yuan and Y. Y. Lu, "Propagating Bloch modes above the lightline on a periodic array of cylinders," J. Phys. B **50**, 05LT01 (2017).
29. Z. Hu and Y. Y. Lu, "Resonances and bound states in the continuum on periodic arrays of slightly noncircular cylinders," J. Phys. B **51**, 035402 (2018).
30. F. Monticone and A. Alu, "Leaky-wave theory, techniques, and applications: from microwaves to visible frequencies," Proc. IEEE **103**, 793–821 (2015).
31. L. Yuan and Y. Y. Lu, "Strong resonances on periodic arrays of cylinders and optical bistability with weak incident waves," Phys. Rev. A **95**, 023834 (2017).
32. L. Yuan and Y. Y. Lu, "Bound states in the continuum on periodic structures surrounded by strong resonances," Phys. Rev. A **97**, 043828 (2018).
33. Q. Bai, M. Perrin, C. Sauvan, J.-P. Hugonin, and P. Lalanne, "Efficient and intuitive method for the analysis of light scattering by a resonant nanostructure," Opt. Express **21**, 27371–27382 (2013).
34. L. Armitage, M. Doost, W. Langbein, and E. Muljarov, "Resonant-state expansion applied to planar waveguides," Phys. Rev. A **89**, 053832 (2014).
35. B. Vial, F. Zolla, A. Nicolet, and M. Commandré, "Quasimodal expansion of electromagnetic fields in open two-dimensional structures," Phys. Rev. A **89**, 023829 (2014).
36. B. Vial and Y. Hao, "A coupling model for quasi-normal modes of photonic resonators," J. Opt. **18**, 115004 (2016).
37. F. Alpeggiani, N. Parappurath, E. Verhagen, and L. Kuipers, "Quasinormal-mode expansion of the scattering matrix," Phys. Rev. X **7**, 021035 (2017).
38. A.-L. Fehrembach, B. Gralak, and A. Sentenac, "Vectorial model for guided-mode resonance gratings," Phys. Rev. A **97**, 043852 (2018).
39. S. Fan, W. Suh, and J. D. Joannopoulos, "Temporal coupled-mode theory for the Fano resonance in optical resonators," J. Opt. Soc. Am. A **20**, 569–572 (2003).
40. W. Suh, Z. Wang, and S. Fan, "Temporal coupled-mode theory and the presence of non-orthogonal modes in lossless multimode cavities," IEEE J. Quantum Electron. **40**, 1511–1518 (2004).
41. R. E. Hamam, A. Karalis, J. D. Joannopoulos, and M. Soljačić, "Coupled-mode theory for general free-space resonant scattering of waves," Phys. Rev. A **75**, 053801 (2007).
42. C. Linton, V. Zalipaev, and I. Thompson, "Electromagnetic guided waves on linear arrays of spheres," Wave Motion **50**, 29–40 (2013).
43. J. Kong, L. Tsang, and K. Ding, *Scattering of Electromagnetic Waves, Theories and Applications* (2000), vol. **1**.
44. E. N. Bulgakov and A. F. Sadreev, "Transfer of spin angular momentum of an incident wave into orbital angular momentum of the bound states in the continuum in an array of dielectric spheres," Phys. Rev. A **94**, 033856 (2016).
45. E. N. Bulgakov and A. F. Sadreev, "Propagating Bloch bound states with orbital angular momentum above the light line in the array of dielectric spheres," J. Opt. Soc. Am. A **34**, 949–952 (2017).
46. E. N. Bulgakov and D. N. Maksimov, "Light enhancement by quasi-bound states in the continuum in dielectric arrays," Opt. Express **25**, 14134 (2017).
47. Z. Ruan and S. Fan, "Temporal coupled-mode theory for light scattering by an arbitrarily shaped object supporting a single resonance," Phys. Rev. A **85**, 043828 (2012).
48. Y. Guo, M. Xiao, and S. Fan, "Topologically protected complete polarization conversion," Phys. Rev. Lett. **119**, 167401 (2017).
49. E. N. Bulgakov and D. N. Maksimov, "Topological bound states in the continuum in arrays of dielectric spheres," Phys. Rev. Lett. **118**, 267401 (2017).
50. J. A. Stratton, *Electromagnetic Theory* (McGraw-Hill, 1941).
51. I. Thompson and C. M. Linton, "Guided surface waves on one- and two-dimensional arrays of spheres," SIAM J. Appl. Math. **70**, 2975–2995 (2010).